Nanotechnology 35 (2024) 175201 (8pp) https://doi.org/10.1088/1361-6528/ad1d78

Lateral junctions of transition metal dichalcogenides as ballistic channels for straintronic applications

Samuel Dechamps[1,*], **Viet-Hung Nguyen**[2] and **Jean-Christophe Charlier**[2]

[1] Université Grenoble Alpes, CEA, IRIG-MEM, 38000 Grenoble, France
[2] Institute of Condensed Matter and Nanosciences, Université catholique de Louvain (UCLouvain), Chemin des étoiles 8, B-1348 Louvain-la-Neuve, Belgium

E-mail: samuel.dechamps@cea.fr, viet-hung.nguyen@uclouvain.be and jean-christophe.charlier@uclouvain.be

Received 25 July 2023, revised 19 November 2023
Accepted for publication 11 January 2024
Published 5 February 2024

Abstract

In the context of advanced nanoelectronics, two-dimensional semiconductors such as transition metal dichalcogenides (TMDs) are gaining considerable interest due to their ultimate thinness, clean surface and high carrier mobility. The engineering prospects offered by those materials are further enlarged by the recent realization of atomically sharp TMD-based lateral junctions, whose electronic properties are governed by strain effects arising from the constituents lattice mismatch. Although most theoretical studies considered only misfit strain, first-principles simulations are employed here to investigate the transport properties under external deformation of a three-terminal device constructed from a $MoS_2/WSe_2/MoS_2$ junction. Large modulation of the current is reported owing to the change in band offset, illustrating the importance of strain on the p–n junction characteristics. The device operation is demonstrated for both local and global deformations, even for ultra-short channels, suggesting potential applications for ultra-thin body straintronics.

Supplementary material for this article is available online

Keywords: quantum transport, straintronics, TDMs lateral junctions

The development of advanced semiconductor technologies relies on the continuous increase in performance of integrated circuits, achieved so far by the miniaturization of their elementary components, mostly field effect transistors (FETs) and diodes [1]. As those conventional devices enter the nanometer regime, this technological growth is facing severe issues, including substantial variation and low reliability of the device parameters, poor gate controllability and short channel effects [2]. In this context, two-dimensional (2D) layered materials such as graphene, hexagonal boron nitride, transition metal dichalcogenides (TMDs), phosphorene, silicene, germanene, stanene, ... [3, 4] are gaining considerable interest. Their ultimate thinness and dangling-bonds-free surface would enable device miniaturization at the atomic scale, while improving electrostatic control and suppressing short channel effects significantly [5].

Among 2D materials, TMDs are promising candidates for electronic applications due to their semiconducting characteristics and high carrier mobility [6, 7]. Single-layer TMDs exhibit a Young's modulus of about 200 GPa [8], greater than most 2D materials, making them appealing candidates for flexible electronics [9]. In addition, TMDs are able to sustain strains of 6%–10% before breaking [10]. The combination of those mechanical features with their tunable electronic properties reflects the enormous prospects of those materials for straintronic applications [11]. In particular, strain was found to tune the carriers mobility [12] and effective mass [13, 14], causing subsequent modulations of the on-state currents in

[*] Author to whom any correspondence should be addressed.

 © 2024 IOP Publishing Ltd

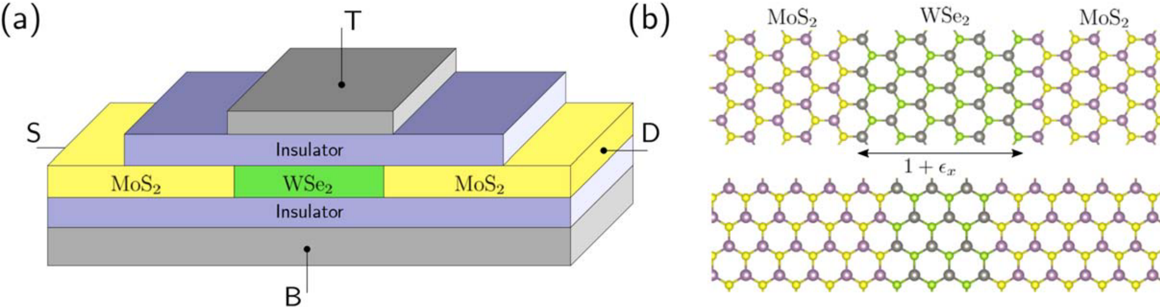

Figure 1. Three-terminal-device based on 2D lateral heterojunctions (a) The elementary transistor is composed of top (T) gate, back (B) gate, source (S), drain (D) and a $MoS_2/WSe_2/MoS_2$ heterojunction as the channel. The lengths of the top gate and the WSe_2 channel are denoted L_g and L_{WSe_2}, respectively. (b) The interface is either zigzag (top) or armchair (bottom), while the WSe_2 strip is strained by an amount $(1 + \epsilon_x)$ along the transport axis.

TMDs transistors [15–17]. Similarly, piezoresistivity was reported in nanoelectromechanical devices [18] due to the band gap sensitivity on strain [19, 20].

The integration of TMDs into developing nanoelectronics is further enlarged when forming heterostructures (HSs), either vertically by stacking single-layers [21–24] or laterally by stitching them together [23–26]. TMD-based vertical HSs have demonstrated great potential for electronic applications, including solar cells [27], complementary metal-oxide-semiconductors [28], p–n diodes [29] and photodetectors [30]. In comparison, lateral HSs exhibit similar p–n junction behaviors such as rectifying properties [31] and photovoltaic effects [32], while displaying higher carriers mobility [33]. As interaction between constituents is stronger and more localized than in their vertical counterparts, those systems provide an exciting one-dimensional platform for quantum engineering [26].

Since dissimilar TMDs always exhibit lattice mismatch, strain effects are unavoidable when forming lateral junctions. While this feature essentially governs interfacial properties such as band alignment or charge redistribution effects [34], it concurrently offers engineering possibilities at the atomic scale. Those prospects are further motivated by recent advances in growth, where remarkable control over sharpness [35, 36] and strain [34, 37, 38] was demonstrated at the interface. In essence, the structure of the junction can be designed in a controllable manner through the type of substrate [34], the supercell dimension [37] or the growth process [38]. On this basis, tunnel FETs based on TMDs lateral HSs were found to be ideal for ultra-low power consumption devices due to the presence of misfit strain [39]. Conversely, the opportunities opened by the application of extrinsic strain in those systems remain yet to be explored.

Strain can be introduced in 2D materials uniaxially by bending or elongating the substrate while piezoelectric stretching or thermal expansion generate biaxial strain [40]. The layer is then deformed globally, with an amplitude of at most 3% when stretching the substrate [41]. Asymmetric strain profiles emerge when those techniques are combined with materials showing different mechanical and thermal properties. In parallel, local strain is applicable through diverse methods such as pressurized blisters, blown-bubble, tip indentation and ripple formation [42]. Alternatively, tuning the substrate protruding features enables precise strain accumulation as the overlaid material conforms to the surface morphology owing to the strong interfacial adhesion [43].

In this work, we investigate the charge transport properties of a three-terminal device constructed from a $MoS_2/WSe_2/MoS_2$ heterojunction (see figure 1(a)), with the WSe_2 channel strained uniaxially along the transport axis. Charge density is modulated in this central region by the top gate voltage (V_{gs}) whereas an electron doping of 5×10^{12} cm^{-2} is imposed in the MoS_2 contacts upon application of a back gate, in agreement with values reported in the literature [44]. At such doping levels (below $10^{13}\,cm^{-2}$), the band structure can be assumed to be shifted rigidly [45]. The current is computed in the ballistic regime using the Landauer formula [46] for a drain-source voltage (V_{ds}) of 0.1 V, based on first-principles simulations performed with *OpenMX* [47–49]. Owing to the impossibility to directly simulate the insulator and the top gate, the analysis is restricted to the subthreshold regime while V_{gs} is modeled as an electric potential (U_g) added to the Hamiltonian. This also means that the fringing of the electric field or quantum capacitance effects are not included in the simulations. Additional information are provided in the supplementary material.

Compared to state-of-the-art simulations, the present computational framework aims at providing an accurate atomic-scale analysis of straintronics in lateral junctions of TMDs, assembled into devices extending over tens of nanometers. The complicated physics of those systems is explicitly described by first-principles methods, as opposed to semi-empirical techniques which require a proper calibration of parameters. Typically, strain effects are included using an effective mass approach [50, 51] or maximally localized Wannier functions [39, 52, 53]. Such models are however fine-tuned on isolated materials, thus disregarding the complex interplay between strain and interfacial effects. Importantly, the role of the latter on the transport properties of strained heterogeneous devices based on 2DMs remains mostly unexplored. Those issues are addressed herein with an intermediate framework that offers an adequate trade-off between accuracy and scaling. In this context, MoS_2–WSe_2 lateral junctions are ideal candidates for investigation using *ab initio* simulations, since their electronic properties differ substantially from their pristine counterparts owing to the

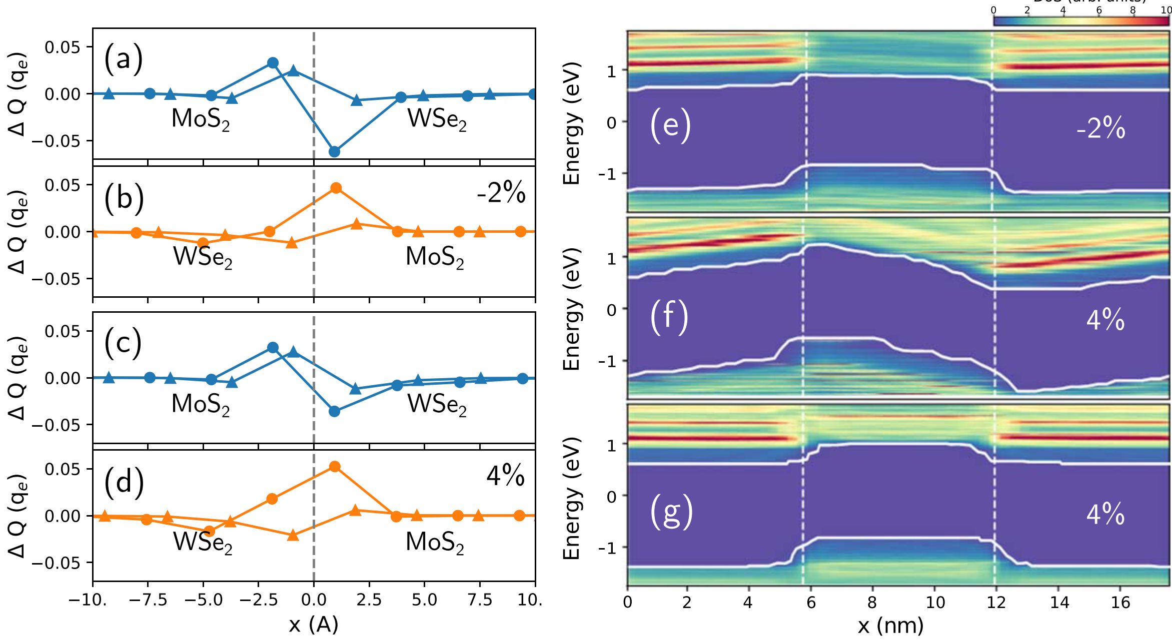

Figure 2. Interfacial properties of MoS_2–WSe_2 lateral junctions. (a)–(d) Excess charge as a function of the distance from the interface (indicated by a dashed line), as obtained from a Mulliken population analysis for the zigzag interface at $\epsilon_x = -2\%$ and $\epsilon_x = 4\%$. The dots and triangles represent M and X atoms, respectively. Local density of states (LDoS) as a function of energy and position along the device length at various strains, for both (e), (f) zigzag and (g) armchair interfaces. The valence and conduction band edges are highlighted in white.

noticeable lattice mismatch and the different chemical compounds involved.

1. Interfacial properties of MoS_2–WSe_2 lateral junctions

Covalent bonding limits the constitutive TMDs to display relatively similar lattice structures, such that a coherent interface is energetically favored. In recent years, it was demonstrated that MoS_2–WSe_2 lateral junctions can be synthesized as atomically sharp semi-coherent interfaces extending over tens of nanometers [34, 36], despite their noticeable lattice mismatch and the different chemical compounds involved. Those last features make this specific junction of particular interest, as demonstrated further. Figure 1(b) illustrates the applied strain profile and the two types of commensurate systems that are considered herewith. Although both zigzag and armchair interfaces are observed experimentally, the former one tends to be the preferable direction for growth [34, 38, 54–56]. Along the junction axis, the WSe_2 strip is constrained to the lattice structure of MoS_2, resulting in a strain of 3.9%.

The relative alignment between the energy bands of TMDs is dictated by the transition metal *d*-orbitals and the chalcogen *p*-orbitals [57], with the position of the bands extrema increasing in energy with the atomic numbers. At the interface, the band offset is affected by the lattice mismatch and the electric dipoles resulting from bonding asymmetries.

Figure 2 presents the excess of charges at the zigzag interface and the junction local density of states (LDoS), illustrating the joint roles of strain and the interface geometry on band offset. First, the amount of charge exchanged is found to depend on the type of covalent bonds at the junction. A net charge gain is observed in MoS_2 as the *d*-orbitals of Mo act as electron accommodators. Conversely, charge accumulation is absent in the armchair configuration as Mo and W atoms form pairs of equivalent bonds. Second, a zigzag interface results in two asymmetric junctions whereas an armchair interface has a two-fold rotational symmetry. This structural (a)symmetry generates a similar (a)symmetry in the charge redistribution. These two discrepancies imply that zigzag and armchair interfaces display contrasting LDoS. At similar strain, the LDoS is found to be symmetric for the armchair interface while an asymmetric band bending occurs for the zigzag one, in agreement with [58, 59]. The band bending slope is dictated by the charge build-up at each interface, as electric dipoles generate a potential gradient along the WSe_2 strip. Strain influences the amount of charge transferred across the junction as well as the band gap of WSe_2, with the former effect altering band bending while the latter affects band offset. The flat bands reported for -2% constitutes a singular case of inversion of the slope sign.

Zhang *et al* [34] used scanning tunneling microscopy to measure the band alignment in MoS_2–WSe_2 lateral junctions grown on a WSe_2 single-layer. The misfit strain was found to induce a type II to type I transition, owing to the band gap reduction in MoS_2. Correspondingly, the valence band offset (VBO) was approximately estimated to 0.65 eV while the conduction band offset (CBO) was determined to be 0.40 eV. From our calculations, the VBO and the CBO for the most stable zigzag configuration ($\epsilon_x = 0.5\%$) are found to be 0.4 eV and 0.22 eV, respectively, yielding a type II heterojunction. This estimation of the VBO is in good agreement with the

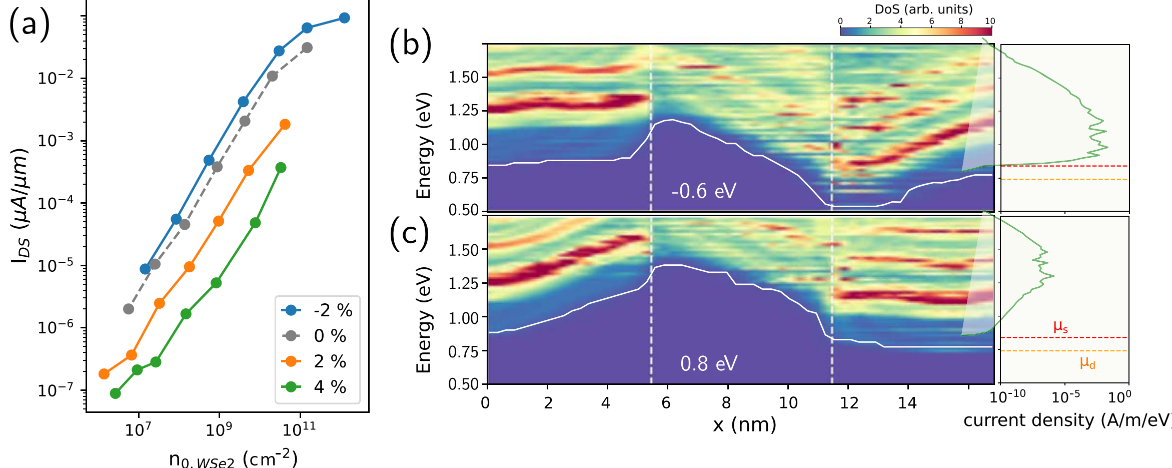

Figure 3. Transport properties of a MoS_2–WSe_2 based three-terminal device. (a) Transfer characteristics for the lateral junctions of MoS_2 with a central strip of WSe_2 for a channel (gate) length of 5.8 nm and an applied bias of $V_{ds} = 0.1$ V. The corresponding LDoS as a function of energy and position along the device length and the current density spectrum, for $\epsilon_x = 4\%$ at (b) $U_g = -0.6$ eV and (c) 0.8 eV. The source and drain quasi-Fermi energies are denoted as μ_s and μ_d, respectively.

theoretical work of Guo *et al* [60], illustrating the strongly pinned nature of lateral systems.

2. Transport properties of MoS_2–WSe_2 lateral junctions

Figure 3(a) displays the current across the junction (I_{ds}) as a function of strain and the carriers density inside the channel ($\tilde{n}_{0,\mathrm{WSe_2}}$), resembling the transfer characteristics of a FET operating ideally in the sub-threshold regime [61]. Within the present computational framework, $\tilde{n}_{0,\mathrm{WSe_2}}$ is preferred to U_g to characterize the channel due to its experimental accessibility using inversion charge measurements from capacitance–voltage characteristics. While this approximation implies that typical transistor parameters (sub-threshold swing, transconductance, ...) are not obtainable, strain-related effects under electrostatic gating are accurately described. For a 5.8 nm channel, strain-tuning of the current is predicted as I_{ds} increases (decreases) with compressive (tensile) strain. Note that the current plateau observed for $\epsilon_x = -2\%$ does not correspond to the saturation regime as doping remains quite low. Lastly, the proper operation of the top gate is illustrated in figures 3(b), (c), where U_g is shown to modulate the energy levels of electronic states located inside the channel.

Owing to the device ultra-short channel, I_{ds} stems for the most part at low doping from quantum tunneling currents instead of thermionic ones. Such simple analytical approach also offers significant insight on the predominance of certain strain-dependent transport features. In the case of a rectangular potential barrier, tunneling transmissions are expressed as

$$T(E) = 1/(\cosh^2(\beta w) + (\gamma/2)^2 \sinh^2(\beta w)) \tag{1}$$

where $\beta^2 = 2m^*(E_b - E)/\hbar^2$, $\gamma = \beta/k - k/\beta$. The barrier width, height and the carriers effective mass are denoted w, E_b and m^*, respectively. First, strain effects on the band structure are represented in figure 4(a), showing an indirect-to-direct transition of the band gap. Consequently, the current is expected to exhibit an energy-dependent distribution between the K and Q valleys. In this analysis, the former contribution is disregarded as electronic transport is demonstrated to originate predominantly from the Q valley (see supplementary information). Second, the strain dependence of the model parameters is depicted in figures 4(b), (c), with w kept as an additional degree of freedom. The band gap (E_g) of strained WSe_2 is provided for comparison with the barrier height, corresponding here to the CBO. An almost identical dependence is reported between the two, in agreement with previous measurements on Schottky barriers for metal-contacted WSe_2 [62], indicating the strain-free character of the VBO and the strongly pinned nature of lateral systems. As concerns m^*, only the radial part is considered here, owing to the equivalent behavior between this latter component and the transverse one [15–17, 63]. Its estimation is in satisfactory agreement with previous theoretical works [63, 64], as m^* is found to increase with uniaxial strain, similarly to the case of biaxial strain in other TMDs [15–17].

Figure 4(d) displays the transmissions obtained from first-principles and the tunneling model, where w is determined to yield the best fit. Interestingly, the analytical model predicts w to decrease with strain, consistently with figures 2(e)–(f). The potential shape changes from rectangular to triangular as strain increases, due to the aforementioned band bending effect. The discrepancy between the channel length and w results most probably from the model simplicity and the assumption of an isotropic effective mass. Lastly, transmissions deviate more for larger deformation due to the diminishing contribution of the Q valleys, causing the wave function to present a more pronounced mixed character. This phenomena generates larger transmissions due to the underlying increase in DoS, as illustrated for $\epsilon_x = 4\%$.

The output characteristics are depicted in figure 5(a) at several gate potentials for both compressive and tensile

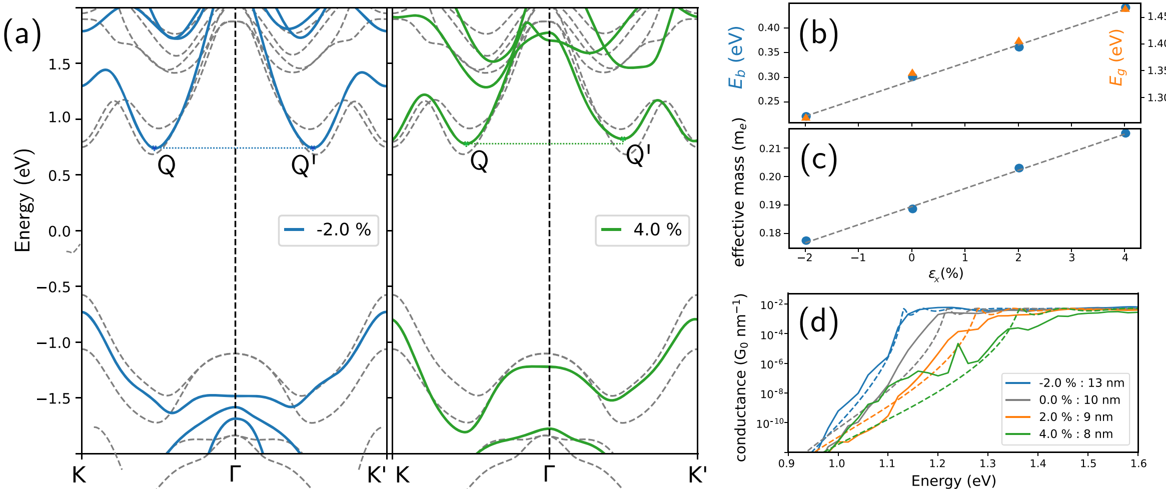

Figure 4. Quantum transport tunneling model. (a) Electronic band structures of strained WSe_2 along the each non-degenerate valleys, with respect to pristine WSe_2 (grey dashed lines) while the Q and Q' valleys bottom are compared (dotted lines). The model parameters are presented as a function of strain, with (b) the band gap (E_g) (orange) compared to the energy barrier height (E_b) at the MoS_2–WSe_2 interface (blue) and (c) the effective mass computed at the Q point. (d) Electronic transmission per unit area as a function of energy for different strain profiles, obtained from first-principles (solid lines) and from the quantum tunneling model (dashed lines). Transmissions are computed at $V_{\mathrm{ds}} = 0.1$ V and $U_g = 0$ eV while the legend in the inset indicates the barrier width.

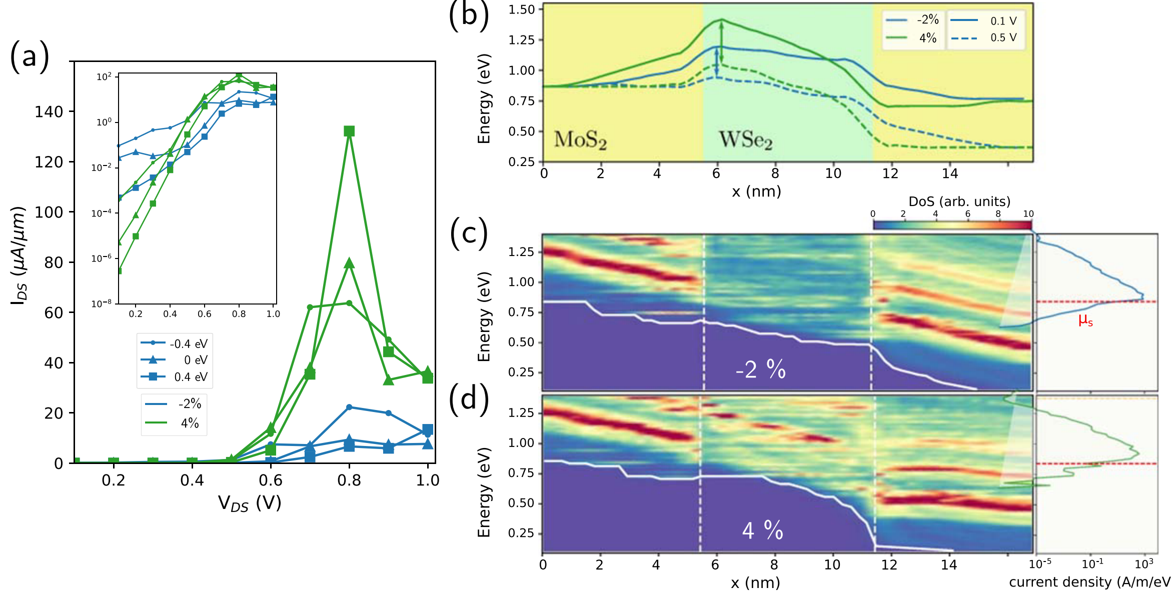

Figure 5. Transport properties of a MoS_2–WSe_2-based three-terminal device as a function of V_{ds}. (a) Output characteristics for various gate potential (U_g) at $\epsilon_x = -2\%$ and 4%; inset: in logarithmic units. (b) The highest conduction band as V_{ds} increases from 0.1 V to 0.5 V, in solid and dashed lines, respectively, when $U_g = 0.4$ eV. The arrows indicate the potential barrier drop. The corresponding LDoS as a function of energy and position along the device length and the current density spectrum when V_{ds} is increased to 0.8 V, for (c) $\epsilon_x = -2\%$ and (d) 4%. The quasi-Fermi energy of the source is denoted as μ_s.

strains. The current is seen to increase exponentially at small voltages (see inset), with a sensitivity on V_{ds} that intensifies with strain. This discrepancy originates from the stronger electric field induced by the larger charge transfer across the junction when $\epsilon_x = 4\%$. The steeper band profile then results in an increased sensitivity of the barrier height, as indicated by the sharper drop in figure 5(b). The linear region is reached once V_{ds} is large enough to compensate for the potential barrier, typically above 0.5 V. The saturation regime is attained after a transition of about $10\,k_{\mathrm{B}}T$, where negative differential resistance is reported in agreement with previous theoretical works [65]. The current non-monotonic behavior stems from strain-induced variations in the channel DoS, as illustrated in figures 5(c), (d). At gate potentials close to 0.8 eV, an improved alignment between incoming and channel states increases the number of modes available for transport. Such effects is greater for tensile strain, in contrast with currents computed in the subthreshold regime for which compressive strain exhibited better transmissions.

It was assumed to this point that the channel and the top gate overlap perfectly, although their lengths would evidently differ in practice. Such discrepancy could then degrade the

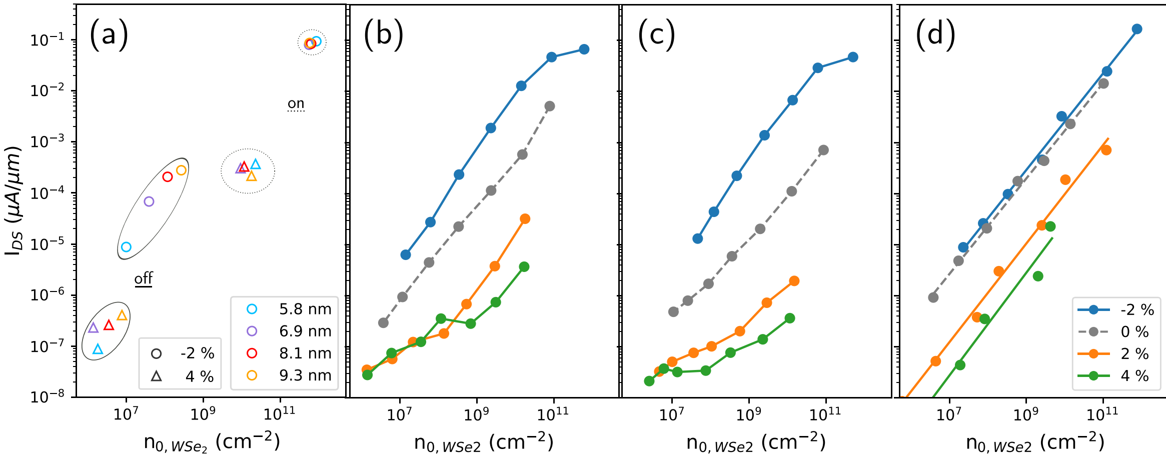

Figure 6. Transport properties of a MoS_2–WSe_2-based three-terminal device depending on the channel length (L_{WSe_2}), gate length (L_g) and strain at $V_{ds} = 0.1$ V. (a) On and off currents in dashed and solid circles, respectively, as L_g increases while $L_{WSe_2} = 5.8$ nm. Transfer characteristics for the device when (b) $L_{WSe_2} = 8.7$ nm and (c) 11.6 nm. (d) Transfer characteristics for the device under uniform uniaxial strain when $L_{WSe_2} = 5.8$ nm.

device performance or impede its proper functioning. To address this concern, the region under electrostatic gating (L_g) is extended beyond the WSe_2 channel. Figure 6(a) presents the on- and off-current values for L_g ranging from 5.8 nm to 9.3 nm, with the on-currents defined when $U_g = -0.4$ eV and the channel fixed at 5.8 nm. It appears that both I_{ds} and n_{0,WSe_2} substantially increase with L_g in the off-state whereas the on-state appears mostly unaffected. While strain-induced current modulation remains, extending the gate beyond the interface reduces the gate controllability for ultra-short channels at low doping due to the greater charge transfer. However, this detrimental effect is expected to subside for longer channels.

Figures 6(b), (c) displays the transfer characteristics for $L_{WSe_2} = 8.7$ nm and 11.6 nm, showing an improved strain-controllabilty when the channel lengthens. The current becomes mostly thermionic as the tunneling contribution dwindles, while observing an almost constant $\tilde{n}_{0,WSe_2}$ evidences its reliability to characterize the carriers statistics inside the channel. It can be assumed from previous theoretical works [39, 66] that other parameters related to the device electrostatic integrity improve as it scales up.

Although some strategies enable to locally strain the system in the channel, the MoS_2 region would in reality be deformed as well. Figure 6(d) presents the current characteristics when the MoS_2 leads are strained uniaxially with the WSe_2 strip, under the requirement that $\tilde{n}_{MoS_2} = 5 \times 10^{12}$ cm^{-2}. A noticeable noise is reported but the strain-controllabity remains overall acceptable. While current modulation is absent for compressive strain due to the ultra-short channel, this feature is well preserved in the more practical case of tensile strain. In this regard, functional operation for global strains represents a decisive advantage of heterojunctions over mono-crystals, where strain-induced current modulation occurs only for local deformations.

Lastly, the impact of defects has been neglected even though their presence at the interface has been observed experimentally [34]. In spite of their fundamental role in strain relaxation mechanisms, defects are not expected to substantially affect the device performance. Indeed, Cao *et al* [67] demonstrated that optoelectronic properties of lateral HS are only minimally affected by interfacial imperfections. On the contrary, those defects could represent an intriguing playground for the design of additional strain-induced transport mechanisms.

3. Conclusion

In summary, a MoS_2–WSe_2 lateral HS is studied by means of first-principles quantum transport simulations. A type-II band alignment is reported, with band bending occurring at the junction vicinity for zigzag interfaces. Strain is observed to significantly influence band alignment by increasing both the band gap in WSe_2 and the charge transfer across the interface. Transport calculations in the zigzag configuration reveal strain-induced current modulation, as tunneling and thermionic transports depend exponentially on the CBO, in contrast with the moderate gain theoretically predicted in n-type MX_2 FETs [15–17]. The device operational robustness is demonstrated for global strain and non-ideal gating profiles while current modulation is shown to improve with the channel length.

This theoretical work represents a preliminary step towards the demonstration of the unique platform that constitutes TMDs lateral junctions. Those systems are at the scaling limit of quantum engineering due to their ultimate thinness and similar chemical environment [68], contrary to mixed-dimensional architectures where WSe_2 is more perturbed [62, 69], while decisively operating at any strain field, in contrast to mono-crystals. In the context of strain sensors, the gauge factor should be estimated, as strain gauges comparable to that of state-of-the-art silicon sensors were already demonstrated for MoS_2 devices [70]. In the scope of low power electronics, one should consider the tunnel FET for its improved sub-thermionic operation, where strain-tuning of

the band alignment would be extremely useful. From a computational perspective, semi-empirical studies based on more advanced Poisson solvers are required, thus providing the device complete transfer characteristics and further insight into its transport mechanisms.

Acknowledgments

The authors acknowledge financial support from the Fédération Wallonie-Bruxelles through the ARC Grants (No 16/21-077 and No 21/26-116), from the European Union's Horizon 2020 Research Project and Innovation ProgramGraphene Flagship Core3 (No 881603), and from the Belgium F.R.S.-FNRS through the research project (No T.0051.18). Computational resources have been provided by the CISM supercomputing facilities of UCLouvain and the CÉCI consortium funded by F.R.S.-FNRS of Belgium (No 2.5020.11).

Data availability statement

The data that support the findings of this study are openly available at the following URL/DOI: https://drive.google.com/drive/u/0/folders/17bIzPPlsTkirm4I-VDPGkhsRAX6m0UNz.

ORCID iDs

Samuel Dechamps https://orcid.org/0000-0002-1657-7926
Viet-Hung Nguyen https://orcid.org/0000-0001-6729-3520

References

[1] Waldrop M M 2016 The chips are down for Moore's law *Nat. News* **530** 144
[2] Kim Y B 2010 Challenges for nanoscale mosfets and emerging nanoelectronics *Trans. Electr. Electron. Mater.* **11** 93–105
[3] Ferrari A C *et al* 2015 Science and technology roadmap for graphene, related two-dimensional crystals, and hybrid systems *Nanoscale* **7** 4598–810
[4] Zeng S, Tang Z, Liu C and Zhou P 2021 Electronics based on two-dimensional materials: status and outlook *Nano Res.* **14** 1752–67
[5] Chhowalla M, Jena D and Zhang H 2016 Two-dimensional semiconductors for transistors *Nat. Rev. Mater.* **1** 16052
[6] Manzeli S, Ovchinnikov D, Pasquier D, Yazyev O V and Kis A 2017 2d transition metal dichalcogenides *Nat. Rev. Mater.* **2** 17033
[7] Radisavljevic B, Radenovic A, Brivio J, Giacometti V and Kis A 2011 Single-layer MoS_2 transistors *Nat. Nanotechnol.* **6** 147–50
[8] Deng S, Li L and Li M 2018 Stability of direct band gap under mechanical strains for monolayer MoS_2, $MoSe_2$, WS_2 and WSe_2 *Physica* E **101** 44–9
[9] Jiang D, Liu Z, Xiao Z, Qian Z, Sun Y, Zeng Z and Wang R 2022 Flexible electronics based on 2d transition metal dichalcogenides *J. Mater. Chem.* A **10** 89–121
[10] Bertolazzi S, Brivio J and Kis A 2011 Stretching and breaking of ultrathin MoS_2 *ACS Nano* **5** 9703–9
[11] Roldán R, Castellanos-Gomez A, Cappelluti E and Guinea F 2015 Strain engineering in semiconducting two-dimensional crystals *J. Phys.: Condens. Matter* **27** 313201
[12] Hosseini M, Elahi M, Pourfath M and Esseni D 2015 Strain-induced modulation of electron mobility in single-layer transition metal dichalcogenides mx2 ($m = mo$, w; $x = s$, se *IEEE Trans. Electron Devices* **62** 3192–8
[13] Kumar A and Ahluwalia P 2013 Mechanical strain dependent electronic and dielectric properties of two-dimensional honeycomb structures of MoX_2 (x = s, se, te) *Physica* B **419** 66–75
[14] Dong L, Namburu R R, O'Regan T P, Dubey M and Dongare A M 2014 Theoretical study on strain-induced variations in electronic properties of monolayer MoS_2 *J. Mater. Sci.* **49** 6762–71
[15] Sengupta A, Ghosh R K and Mahapatra S 2013 Performance analysis of strained monolayer MoS_2 mosfet *IEEE Trans. Electron Devices* **60** 2782–7
[16] Mohammad Tabatabaei S, Noei M, Khaliji K, Pourfath M and Fathipour M 2013 A first-principles study on the effect of biaxial strain on the ultimate performance of monolayer MoS_2-based double gate field effect transistor *J. Appl. Phys.* **113** 163708
[17] Harada N, Sato S and Yokoyama N 2014 Computational study on electrical properties of transition metal dichalcogenide field-effect transistors with strained channel *J. Appl. Phys.* **115** 034505
[18] Jiang D, Liu Z, Xiao Z, Qian Z, Sun Y, Zeng Z and Wang R 2022 Flexible electronics based on 2d transition metal dichalcogenides *J. Mater. Chem.* A **10** 89–121
[19] Johari P and Shenoy V B 2012 Tuning the electronic properties of semiconducting transition metal dichalcogenides by applying mechanical strains *ACS Nano* **6** 5449–56
[20] Ghorbani-Asl M, Borini S, Kuc A and Heine T 2013 Strain-dependent modulation of conductivity in single-layer transition-metal dichalcogenides *Phys. Rev.* B **87** 235434
[21] Geim A K and Grigorieva I V 2013 Van der waals heterostructures *Nature* **499** 419–25
[22] Novoselov K, Mishchenko O A, Carvalho O A and Neto A C 2016 2d materials and van der waals heterostructures *Science* **353** aac9439
[23] Li M Y, Chen C H, Shi Y and Li L J 2016 Heterostructures based on two-dimensional layered materials and their potential applications *Mater. Today* **19** 322–35
[24] Zhang S, Liu J, Kirchner M M, Wang H, Ren Y and Lei W 2021 Two-dimensional heterostructures and their device applications: progress, challenges and opportunities—review *J. Phys. D: Appl. Phys.* **54** 433001
[25] Ling X *et al* 2016 Parallel stitching of 2d materials *Adv. Mater.* **28** 2322–9
[26] Ávalos-Ovando O, Mastrogiuseppe D and Ulloa S E 2019 Lateral heterostructures and one-dimensional interfaces in 2d transition metal dichalcogenides *J. Phys.: Condens. Matter* **31** 213001
[27] Furchi M M, Pospischil A, Libisch F, Burgdörfer J and Mueller T 2014 Photovoltaic effect in an electrically tunable van der waals heterojunction *Nano Lett.* **14** 4785–91
[28] Yu W J, Li Z, Zhou H, Chen Y, Wang Y, Huang Y and Duan X 2013 Vertically stacked multi-heterostructures of layered materials for logic transistors and complementary inverters *Nat. Mater.* **12** 246–52
[29] Cheng R, Li D, Zhou H, Wang C, Yin A, Jiang S, Liu Y, Chen Y, Huang Y and Duan X 2014 Electroluminescence and photocurrent generation from atomically sharp WSe_2/MoS_2 heterojunction p–n diodes *Nano Lett.* **14** 5590–7
[30] Deng Y, Luo Z, Conrad N J, Liu H, Gong Y, Najmaei S, Ajayan P M, Lou J, Xu X and Ye P D 2014 Black phosphorus-monolayer MoS_2 van der waals heterojunction p–n diode *ACS Nano* **8** 8292–9

[31] Chamlagain B, Withanage S S, Johnston A C and Khondaker S I 2020 Scalable lateral heterojunction by chemical doping of 2d tmd thin films *Sci. Rep.* **10** 12970

[32] Wu W, Zhang Q, Zhou X, Li L, Su J, Wang F and Zhai T 2018 Self-powered photovoltaic photodetector established on lateral monolayer MoS_2-WS_2 heterostructures *Nano Energy* **51** 45–53

[33] Zhu J, Li W, Huang R, Ma L, Sun H, Choi J H, Zhang L, Cui Y and Zou G 2020 One-pot selective epitaxial growth of large WS_2/MoS_2 lateral and vertical heterostructures *J. Am. Chem. Soc.* **142** 16276–84

[34] Zhang C, Li M Y, Tersoff J, Han Y, Su Y, Li L J, Muller D A and Shih C K 2018 Strain distributions and their influence on electronic structures of WSe_2-MoS_2 laterally strained heterojunctions *Nat. Nanotechnol.* **13** 152–8

[35] Zhang Z, Chen P, Duan X, Zang K, Luo J and Duan X 2017 Robust epitaxial growth of two-dimensional heterostructures, multiheterostructures, and superlattices *Science* **357** 788–92

[36] Sahoo P K, Memaran S, Xin Y, Balicas L and Gutiérrez H R 2018 One-pot growth of two-dimensional lateral heterostructures via sequential edge-epitaxy *Nature* **553** 63–7

[37] Xie S *et al* 2018 Coherent, atomically thin transition-metal dichalcogenide superlattices with engineered strain *Science* **359** 1131–6

[38] Kobayashi Y, Yoshida S, Maruyama M, Mogi H, Murase K, Maniwa Y, Takeuchi O, Okada S, Shigekawa H and Miyata Y 2019 Continuous heteroepitaxy of two-dimensional heterostructures based on layered chalcogenides *ACS Nano* **13** 7527–35

[39] Choukroun J, Pala M, Fang S, Kaxiras E and Dollfus P 2018 High performance tunnel field effect transistors based on in-plane transition metal dichalcogenide heterojunctions *Nanotechnology* **30** 025201

[40] Roldán R, Castellanos-Gomez A, Cappelluti E and Guinea F 2015 Strain engineering in semiconducting two-dimensional crystals *J. Phys.: Condens. Matter* **27** 313201

[41] Schmidt R, Niehues I, Schneider R, Drueppel M, Deilmann T, Rohlfing M, De Vasconcellos S M, Castellanos-Gomez A and Bratschitsch R 2016 Reversible uniaxial strain tuning in atomically thin WSe_2 *2D Mater.* **3** 021011

[42] Deng S, Sumant A V and Berry V 2018 Strain engineering in two-dimensional nanomaterials beyond graphene *Nano Today* **22** 14–35

[43] Li H *et al* 2015 Optoelectronic crystal of artificial atoms in strain-textured molybdenum disulphide *Nat. Commun.* **6** 1–7

[44] Ye J, Zhang Y J, Akashi R, Bahramy M S, Arita R and Iwasa Y 2012 Superconducting dome in a gate-tuned band insulator *Science* **338** 1193–6

[45] Zhao P, Yu J, Zhong H, Rösner M, Katsnelson M I and Yuan S 2020 Electronic and optical properties of transition metal dichalcogenides under symmetric and asymmetric field-effect doping *New J. Phys.* **22** 083072

[46] Landauer R 1970 Electrical resistance of disordered one-dimensional lattices *Philos. Mag.* **21** 863–7

[47] Ozaki T 2003 Variationally optimized atomic orbitals for large-scale electronic structures *Phys. Rev.* B **67** 155108

[48] Ozaki T and Kino H 2004 Numerical atomic basis orbitals from h to kr *Phys. Rev.* B **69** 195113

[49] Ozaki T 2007 Continued fraction representation of the fermi-dirac function for large-scale electronic structure calculations *Phys. Rev.* B **75** 035123

[50] Alam K 2020 Physical insight and performance metrics of monolayer mx2 heterojunction tfets *Micro Nano Lett.* **15** 81–5

[51] Lucchesi L, Calogero G, Fiori G and Iannaccone G 2021 Ballistic two-dimensional lateral heterojunction bipolar transistor *Phys. Rev. Res.* **3** 023158

[52] Fang S, Carr S, Cazalilla M A and Kaxiras E 2018 Electronic structure theory of strained two-dimensional materials with hexagonal symmetry *Phys. Rev.* B **98** 075106

[53] Marin E G, Marian D, Perucchini M, Fiori G and Iannaccone G 2020 Lateral heterostructure field-effect transistors based on two-dimensional material stacks with varying thickness and energy filtering source *ACS Nano* **14** 1982–9

[54] Zhang X Q, Lin C H, Tseng Y W, Huang K H and Lee Y H 2015 Synthesis of lateral heterostructures of semiconducting atomic layers *Nano Lett.* **15** 410–5

[55] Gong Y *et al* 2014 Vertical and in-plane heterostructures from WS_2/MoS_2 monolayers *Nat. Mater.* **13** 1135–42

[56] Li M Y *et al* 2015 Epitaxial growth of a monolayer WSe_2-MoS_2 lateral pn junction with an atomically sharp interface *Science* **349** 524–8

[57] Kang J, Tongay S, Zhou J, Li J and Wu J 2013 Band offsets and heterostructures of two-dimensional semiconductors *Appl. Phys. Lett.* **102** 012111

[58] Wei W, Dai Y, Sun Q, Yin N, Han S, Huang B and Jacob T 2015 Electronic structures of in-plane two-dimensional transition-metal dichalcogenide heterostructures *Phys. Chem. Chem. Phys.* **17** 29380–6

[59] Wei W, Dai Y, Niu C and Huang B 2015 Controlling the electronic structures and properties of in-plane transition-metal dichalcogenides quantum wells *Sci. Rep.* **5** 1–9

[60] Guo Y and Robertson J 2016 Band engineering in transition metal dichalcogenides: stacked versus lateral heterostructures *Appl. Phys. Lett.* **108** 233104

[61] Ma N and Jena D 2015 Carrier statistics and quantum capacitance effects on mobility extraction in two-dimensional crystal semiconductor field-effect transistors *2D Mater.* **2** 015003

[62] Shen T, Penumatcha A V and Appenzeller J 2016 Strain engineering for transition metal dichalcogenides based field effect transistors *ACS Nano* **10** 4712–8

[63] Kormányos A, Burkard G, Gmitra M, Fabian J, Zólyomi V, Drummond N D and Fal'ko V 2015 k. p theory for two-dimensional transition metal dichalcogenide semiconductors *2D Mater.* **2** 022001

[64] Liu W, Cao W, Kang J and Banerjee K 2013 High-performance field-effect-transistors on monolayer-WSe_2 *ECS Trans.* **58** 281

[65] Bruce A V, Liu S, Fry J N and Cheng H P 2020 Insights into negative differential resistance in MoS_2 esaki diodes: a first-principles perspective *Phys. Rev.* B **102** 115415

[66] Logoteta D, Cao J, Pala M, Dollfus P, Lee Y and Iannaccone G 2020 Cold-source paradigm for steep-slope transistors based on van der waals heterojunctions *Phys. Rev. Res.* **2** 043286

[67] Cao Z, Harb M, Lardhi S and Cavallo L 2017 Impact of interfacial defects on the properties of monolayer transition metal dichalcogenide lateral heterojunctions *J. Phys. Chem. Lett.* **8** 1664–9

[68] Iannaccone G, Bonaccorso F, Colombo L and Fiori G 2018 Quantum engineering of transistors based on 2d materials heterostructures *Nat. Nanotechnol.* **13** 183–91

[69] Jariwala D, Marks T J and Hersam M C 2017 Mixed-dimensional van der Waals heterostructures *Nat. Mater.* **16** 170–81

[70] Manzeli S, Allain A, Ghadimi A and Kis A 2015 Piezoresistivity and strain-induced band gap tuning in atomically thin MoS_2 *Nano Lett.* **15** 5330–5